The amyloid cascade hypothesis and Alzheimer's disease: A mathematical model

M. BERTSCH[1,2], B. FRANCHI[3], L. MEACCI[4], M. PRIMICERIO[2,5] and M.C. TESI[3]

[1]*Dipartimento di Matematica, Università di Roma 'Tor Vergata', Via della Ricerca Scientifica 1, 00133 Roma, Italy*
e-mail: bertsch@mat.uniroma2.it
[2]*Istituto per le Applicazoni del Calcolo 'M. Picone', Consiglio Nazionale delle Ricerche, Via dei Taurini 19, 00185 Roma, Italy*
[3]*Dipartimento di Matematica, Università di Bologna, Piazza di Porta S. Donato 5, 40126 Bologna, Italy*
e-mails: bruno.franchi@unibo.it; mariacarla.tesi@unibo.it
[4]*Instituto de Ciências Matemáticas e de Computação, ICMC, Universidade de São Paulo, Avenida Trabalhador Sancarlense, 400, São Carlos (SP), CEP 13566-590, Brazil*
e-mail: luca.meacci@usp.br
[5]*Dipartimento di Matematica 'U. Dini', Università degli Studi di Firenze, Viale Giovanni Battista Morgagni, 67/A, 50134 Firenze, Italy*
e-mail: mario.primicerio@math.unifi.it

The paper presents a conceptual mathematical model for Alzheimer's disease (AD). According to the so-called amyloid cascade hypothesis, we assume that the progression of AD is associated with the presence of soluble toxic oligomers of beta-amyloid. Monomers of this protein are produced normally throughout life, but a change in the metabolism may increase their total production and, through aggregation, ultimately results in a large quantity of highly toxic polymers. The evolution from monomeric amyloid produced by the neurons to senile plaques (long and insoluble polymeric amyloid chains) is modelled by a system of ordinary differential equations (ODEs), in the spirit of the Smoluchowski equation. The basic assumptions of the model are that, at the scale of suitably small representative elementary volumes (REVs) of the brain, the production of monomers depends on the average degradation of the neurons and in turn, at a much slower timescale, the degradation is caused by the number of toxic oligomers. To mimic prion-like diffusion of the disease in the brain, we introduce an interaction among adjacent REVs that can be assumed to be isotropic or to follow given preferential patterns. We display the results of numerical simulations which are obtained under some simplifying assumptions. For instance, the amyloid cascade is modelled by just three ordinary differential equations (ODEs), and the simulations refer to abstract 2D domains, simplifications which can be easily avoided at the price of some additional computational costs. Since the model is suitably flexible to incorporate other mechanisms and geometries, we believe that it can be generalised to describe more realistic situations.

Key words: Smoluchowski equations, mathematical models of Alzheimer's disease, amyloid cascade hypothesis

2020 Mathematics Subject Classification: Primary: 92C50; 92B05. Secondary: 92C20.

1 Introduction

Alzheimer's disease (AD), a neurodegenerative disease with a huge social and economic impact, is the prevalent form of late-life dementia [36]. The biomedical knowledge about the AD-pathology is rapidly growing, as witnessed by a vast literature, but the aetiology, the mechanisms and the progression of the AD-pathology, as well as their relationship to clinical and cognitive manifestations, are still far from understood. The trajectories of AD-progression in the patient's brain are highly stereotyped but vary individually. The lack of full understanding of the patho-physiology of AD-progression, its insidious onset and the clinical heterogeneity and variability in speed and pattern progression severely complicates the rigorous characterisation and prognosis of the disease and hampers informed, data-driven clinical intervention.

In this context, there is a pressing need to find and validate biomarkers to track and predict disease progression. Several biomarkers are currently under investigation: genetic analysis (Apolipoprotein E status, presenilin and amyloid precursor protein (APP)), cerebrospinal fluid homogenates (CSF tau protein, amyloid $A\beta_{42}$ protein), imaging (atrophy, glucose Positron Emission Tomography (PET) for hypometabolism, AV45-PET for amyloid, T807- or AV1451-PET for tau) and cognitive tests (Alzheimer's Disease Assessment Scale cognitive, Auditory-Verbal Learning Test and Mini-Mental State Exam).

In this paper, we use the *in silico* approach, based on mathematical modelling and computer simulations, and supplementary to the huge amount of *in vivo* and *in vitro* research (see [29, 15, 59, 45, 19, 1, 34, 26, 5, 7, 10]; we refer in particular to [10] for a comprehensive updated overview of mathematical approaches in the literature).

The general idea is to develop a highly flexible model of the interplay between the excess of $A\beta_{42}$ protein in the central nervous system (CNS) and the progression of the disease, focussing on the early stage of the disease where there is still hope to intervene and stop the further development of the disease. Flexibility of the model is essential: it means that one can test several modelling hypotheses based on medical input and easily adapt the model to new medical insight.

Roughly speaking, the $A\beta$ protein is normally produced during life by neurons in the CNS through intramembranous proteolysis of APP, a large trans-membrane protein involved in signal transduction pathways [47]. By unknown and partially genetic reasons, some neurons – referred to as *malfunctioning neurons* – present an unbalance between produced and cleared $A\beta$. This ultimately leads to the presence of highly toxic oligomers of, among other isoforms, $A\beta_{40}$ and $A\beta_{42}$. For the sake of simplicity, from now on we shall write $A\beta$.

More precisely, $A\beta$ oligomers are subject to two different phenomena:

- agglomeration, leading eventually to the formation of long, insoluble amyloid fibrils, which accumulate in spherical microscopic deposits known as senile plaques;
- diffusion through the microscopic tortuosity of the brain tissue.

In addition, recently it has been proposed that neuronal damage spreads in the neuronal net through a neuron-to-neuron prion-like propagation mechanism [9, 53].

Agglomeration can be articulated in several steps [12, 48]: initial *seeds*, soluble small oligomers, protofibrils and insoluble polymers, and amyloid fibrils with a β-sheet conformation. However, this level of description is beyond the scope of our model, as will be explained in detail in the next section. The connection between $A\beta$ and AD relies on the fact that, as is largely

accepted, Aβ amyloid plays an important role in the process of the cerebral damage (the so-called *amyloid cascade hypothesis* [39]). In particular, some *soluble* Aβ_{42} oligomers have been suggested as the principal cause of neuronal death and eventually dementia [60].

Soluble Aβ shows a multiple neurotoxic effect: it induces a general inflammation that activates the microglia which in turn secretes proinflammatory innate cytokines [31] and, at the same time, increases intracellular calcium levels [29], which ultimately leads to apoptosis and neuronal death.

Although senile plaques are associated with AD, their presence is not strictly related to the severity of the disease. High levels of soluble Aβ correlate better with the presence and degree of cognitive deficits than plaque statistics. Indeed, diffuse amyloid plaques are commonly present in the brains of cognitively intact elderly people. Some authors (see, for instance, [32]) overturn the traditional perspective and claim that large aggregates of Aβ can actually be inert or even protective to healthy neurons. Analogously, Aβ monomers have been shown to lack neurotoxicity [56] and have in fact been suggested to be neuroprotective [63, 28].

In the present paper, we introduce a model to describe the toxic effect of beta-amyloid on neurons. Proceeding in the spirit of mean field approximation, we divide a given cerebral region into a number of smaller subregions. In each of them, we write a system of ODEs to describe the evolution of the number of beta-amyloid monomers, oligomers and plaques. These equations depend on the average health state of the neurons in the subregion under consideration, which is updated at given times (say every half a year, a relatively 'long' period which reflects the slow evolution of the disease). The updating depends on both the amount of toxic oligomers which are present in the subregion itself and the average health state in neighbouring subregions. We present some numerical simulations to illustrate the behaviour of solutions and their parameter dependence.

We stress again that the present model only takes into account the evolution of the Aβ and ignores the role played by the microglia in neuronal death and in the formation of senile plaques. For these aspects, we refer, for instance, to [42] and [19]. In the same spirit, we ignore also the progressive degeneration of the brain due to ageing.

The paper is organised as follows. In Section 2, we briefly review some of the mathematical models of AD and in Section 3, we present the basic model. In Section 4, we discuss a specific example of the model and present numerical simulations. We also provide the corresponding source MATLAB codes, which are available in GitHub repository at the URL: https://github.com/LucaMeacci/Alzheimer_MathModel_Ejam. Finally, in the Appendix, existence, positivity and asymptotic behaviour of the example introduced in Section 4 are discussed.

2 Mathematical modelling

The mathematical model of aggregation and diffusion of Aβ analysed in the present paper is based on the so-called Smoluchowski coagulation equations, originally introduced by Smoluchowski [57] in 1917 to describe the binary coagulation of colloidal particles moving according to Brownian motion. Subsequently, these equations were used to model a variety of phenomena such as the evolution of a system of solid or liquid particles suspended in a gas (in aerosol science), polymerisation (in chemistry), aggregation of colloidal particles (in physics), formation of stars and planets (in astrophysics), red blood cell aggregation (in haematology) and behaviour of fuel mixtures in engines (in engineering). Moreover, several additional physical processes have been subsequently incorporated into the model (diffusion, fragmentation,

condensation, influence of external fields, see, e.g., [16, 40, 62]). We refer also to [17, 18] and [1, 5, 7, 23, 35] for a more exhaustive account of the literature on the Smoluchowski system.

In spite of the large literature on applications of Smoluchowski equations in many branches of science, in the field of biomedical research, their use seems to be rather limited. Here, we only consider the applications of coagulation equations to mathematical models related to AD. For different approaches, in particular to prion-like diffusion and role of the tau protein, we refer the reader to [10].

As far as we know, Murphy and Pallitto [45, 49] were the first ones who used Smoluchowski equations to describe Aβ-agglomeration, starting from an *in vitro* approach. More recently, a systematic approach to the modelling of Aβ-agglomeration and the formation of senile plaques was carried on in a series of papers [1, 25, 5, 8, 7, 23, 24, 22, 11, 14]. In [1, 25, 11], the authors consider a model at microscopic scale. They use suitable Smoluchowski-type equations to describe the diffusion and agglomeration of soluble Aβ-oligomers of different lengths in small portion of the cerebral parenchyma, of the size of the soma of a single neuron (from 4 to 100 µm) and the formation of plaques, identified with insoluble assemblies of very long polymers. Some other phenomena were also included in the model, such as fragmentation of long polymers [25] and clearance of Aβ from the CSF [11].

A macroscopic model was proposed in [5, 8]. The authors couple the set of truncated Smoluchowski equations already used in [1] to a kinetic-type transport equation that models the spreading of neuronal damage, including the possibility of spreading through neuron-to-neuron prion-like transmission. The model takes into account both the microscopic phenomena of diffusion and aggregation of the Aβ peptide, characterised by a short timescale (of a few days, the time needed for the formation of the senile plaques: see [42]) and the macroscopic spreading of the disease and the associated cerebral atrophy in large parts of the brain, with a long timescale (of several years, the time needed for the development of the disease). Remarkably, the model involves mathematical quantities (concentration of plaques, neuronal damage) that have a precise counterpart in terms of clinically observed parameters through PIB-PET (Pittsburgh compound-B, to detect senile plaques: see, e.g., [13]) and FDG-PET (fluorodeoxyglucose PET, to evaluate the brain metabolism of both glucose and oxygen: see, e.g., [43]).

Finally, the papers [7, 23, 24, 22] are dedicated to the transition from the microscopic scale to the macroscopic scale, through different mathematical procedures: [7] adapts arguments from modern Boltzmann-type kinetic theory for multi-agent systems [50], while [23, 24, 22] rely on homogenisation procedures (in [23, 24], neurons are assumed to be periodically distributed, whereas [22] introduces randomness of the distributions of neurons and the onset of the disease).

Recently, the production of the Aβ and then the onset of AD have been associated with the tau protein, a prion-like intra-neuronal protein (see, e.g., [38]; we refer to [58] for a careful overview of the subject). Therefore, also the mathematical modelling of prion-like proteins could be relevant to Aβ modelling. We refer, for instance, to [30, 34, 52], but we refer once more to [10] for an exhaustive panorama of the literature.

In most of the previous papers, the diffusion of the amyloid as well as the (possible) prion-type infection is assumed to be uniform, whereas it has been observed that, if we are looking to a real macroscopic model, the disease diffuses between different regions of the brain according to the anatomical connection strength between them. To describe this kind of diffusion, a network model has been introduced in [41, 53, 54, 20, 55, 61, 21].

3 The model

As we explained in the Introduction, our basic assumption is that the progression of AD is related to the evolution of the amount of Aβ in the cerebrospinal fluid (CSF). Amyloids are produced as monomers by neurons, diffuse in the CSF (with a diffusivity that decreases with their size) and may aggregate and polymerise, producing longer polymeric chains. In polymerisation [16, 40, 62], the use of the Smoluchowski equation can be described as follows. For $k \in \mathbb{N}$, let P_k denote a polymer of length k, formed by k identical units (monomers). If the polymers are sufficiently close, they can merge into a single polymer whose length equals the sum of the lengths of the two (only binary reactions are considered). The merge of a polymer of size k with a polymer of size j can be written as

$$P_k + P_j \longrightarrow P_{k+j}.$$
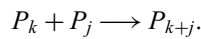
We postulate that there exists a number n such that polymers of length $< n$ are soluble and those of length $\geq n$ are immobile. In the spirit of the dynamics of continuous media, we adopt a strategy of *mean field approximation* and divide the cerebral region under consideration in a sufficiently large number of elements (*representative elementary volumes* (REV)). A more precise discussion on the dimension of the REV will be presented when we will introduce the concept of 'cerebral degradation'. We denote by $w_i(t)$ the number of soluble amyloid polymers of length i ($i < n$) contained in the given REV at time t, while $W_n(t)$ will denote the total number of immobile particles in the REV.

For the sake of simplicity, we assume that there exists a constant $K > 0$ which does not depend on i and j such that the aggregation rate $R_{i,j}$ of two soluble polymers of length i and j is given by

$$R_{i,j} = \begin{cases} K w_i w_j & \text{if } i, j < n, i \neq j \\ \frac{1}{2} K w_i (w_i - 1) \approx \frac{1}{2} K w_i^2 & \text{if } i, j < n, i = j. \end{cases} \tag{3.1}$$

Similarly, assuming that two immobile polymers do not merge, we postulate that the aggregation rate for a soluble and an immobile polymer is given by

$$R_{i,n} = R_{n,i} = K^* w_i W_n \quad \text{if } i < n. \tag{3.2}$$

Since the probability of merging is smaller if one of the two polymers is immobile, we assume that $K^* < K$.

The evolution of the number of monomers in a given REV is described by the differential equation

$$\frac{dw_1}{dt} = -K w_1 \sum_{j=1}^{n-1} w_j - K^* w_1 W_n + \Lambda - M_1 w_1, \tag{3.3}$$

where $\Lambda > 0$ is the production rate of monomers and $M_1 > 0$ their mortality, that is, the clearance due to both the phagocytic activity of the microglia and the possible reabsorption by blood vessels (see [51, 2]). The evolution of the number of oligomers, $w_s(t)$ with $1 < s < n$, is described by

$$\frac{dw_s}{dt} = \frac{K}{2} \sum_{i+j=s} w_i w_j - K w_s \sum_{j=1}^{n-1} w_j - K^* w_s W_n - M_s w_s. \tag{3.4}$$

Finally, the differential equation for the number of immobile aggregates is

$$\frac{dW_n}{dt} = \frac{K}{2} \sum_{i+j \geq n;\, i,j < n} w_i w_j - M_n W_n. \tag{3.5}$$

The next step is to model the progression of AD. We associate the average degree of malfunctioning of the neurons in each REV with a parameter a ranging from 0 to 1; $a = 0$ means that this portion of the brain is healthy, while $a = 1$ corresponds to complete degeneration. At this point, we discuss the dimension of the REV. It should be large enough to contain a sufficiently large number of neurons so that it makes sense to define the quantity a as the average degree of malfunctioning of the neurons contained in the REV. On the other hand, the dimensions of the REV are to be taken small enough so that the variation of a over the macroscopic scale of the cerebral region is identifiable. Ideally, the experimental resolution of the FDG-PET, extensively discussed in [44], should suggest how to choose the size of the REV, which could very well depend on the part of the brain under consideration. In reality, the size of the REV is also determined by computational costs, an issue which becomes of critical importance in the case of 3D simulations. For each REV, we assume that a is a nondecreasing function of time, and its variation is essentially due to two different effects:

- a *local effect*, due to the level of toxicity of the amyloids in the REV itself;
- a *non-local effect*, induced by degradation of the adjacent REVs.

Concerning the local effect, the current opinion is that, while monomers are innocuous, neurons degenerate if the concentration of soluble toxic oligomers exceeds a given threshold. The relative influence $\gamma_i > 0$ of each oligomer is still under investigation, but we can define the quantity

$$D = \sum_{i=2}^{n-1} \gamma_i w_i, \tag{3.6}$$

and assume that degradation occurs when D exceeds a threshold value $D^* > 0$.

Since the typical timescale of degradation is much slower than that of aggregation, it is reasonable to assume that there exists $T > 0$ such that a is constant in each of the time intervals $(0, T)$, $(T, 2T)$, $(2T, 3T)$, ..., and update the value of a at the times $T, 2T, 3T$, etc. Typically, $(0, T)$ can be thought of as a period of half a year.

Based on these considerations, we postulate for the local effect the relation

$$a(t) = a(mT) + \theta[D(mT) - D^*]_+ \quad \text{for } mT < t \leq (m+1)T, \tag{3.7}$$

where $[\cdot]_+$ means the positive part and θ is a given positive constant.

To model the non-local effect, we assume that the REVs in which we divide the cerebral region under investigation are cubes of equal size stacked in such a way that each of them has faces in common with its neighbours. We define the neighbourhood of an REV (located in the interior of the region) as formed by the 26 cubes that have at least one vertex in common with it. If we consider the region embedded in a 'virtual frame' formed by cubes where a is constantly equal to zero, the definition applies to every REV to be considered. At this point, we update the value of a in the following way:

$$a(t) = a(mT) + \sigma \sum [a_k(mT) - a(mT)]_+ \quad \text{for } mT < t \leq (m+1)T, \tag{3.8}$$

where the sum ranges over the 26 cubes in the neighbourhood of the given REV, and σ is a given positive constant. Condition (3.8) can be easily generalised. For example, we could assume that the influence of the neighbours is different in different directions, that is, substituting the sum on the RHS by $\sum \sigma_k [a_k(mT) - a(mT)]_+$.

Combining (3.7) and (3.8), we obtain the law by which we update the value of a in each REV of the region at times $T, 2T, 3T$, etc.

The final step in the modelling consists in specifying how the level of degeneration influences the dynamics of the amyloids. The influence is twofold: on the one side, the degeneration leads to the reduction of the number of 'active' neurons, but, on the other side, it also causes an increased production of monomers by each neuron. Combining the two effects, we can postulate that the number of monomers produced in the REV per unit time is given by

$$\Lambda = A(1-a)(1+\beta a), \tag{3.9}$$

where A is the number of monomers produced in a healthy REV and $\beta > 1$ is a prescribed constant. It is known that, during the disease, the maximum production of amyloid can be of 4–6 times larger than in a healthy brain (see, e.g., [19]). Accordingly, we choose $\beta = 15$.

4 A specific example

To test the model, we consider the following simplified situation: we divide the total population of amyloids into just three subpopulations: monomers, toxic oligomers and immobile aggregates (a larger number of subpopulations just requires a more cumbersome notation and only leads to a slight increase in computing time and a less transparent visualisation of the results).

We rescale w_i $(i = 1, 2, 3)$ by a number N to be chosen and define

$$X(t) = \frac{w_1(t)}{N}, \quad Y(t) = \frac{w_2(t)}{N}, \quad Z(t) = \frac{w_3(t)}{N}.$$

According to [46], the mass of a monomer is about 4.5 kDa, that is, about 8×10^{-12} nanograms. We choose $N = 10^{11}$, corresponding to the order of magnitude of the number of monomers in a nanogram, so that X represents, in order of magnitude, the mass of monomers in nanograms in the REV. For the evolution of the amyloids, we choose *one day* as the unit time.

Setting $k = KN, k^* = K^*N$ and $\lambda = \Lambda/N$, the differential equations (3.3–3.5) take the form

$$\begin{cases} X' = -kX^2 - kXY - k^*XZ - M_1X + \lambda \\ Y' = \frac{1}{2}kX^2 - kXY - kY^2 - k^*YZ - M_2Y \\ Z' = \frac{1}{2}kY^2 + kXY - M_3Z. \end{cases} \tag{4.1}$$

The production rate Λ is given by (3.9) where the constant A represents the production rate in a healthy tissue. Rescaling yields

$$\lambda = \lambda_0(1-a)(1+\beta a) \qquad \text{with } \lambda_0 = A/N.$$

We observe that the production rate λ_0 depends on the total number of REVs used to describe the brain. Here, we assume that we have about 500 REVs of equal size. Choosing $\lambda_0 = 2$ corresponds to a daily monomer production of 2 nanograms in each REV and 1000 nanograms in a healthy brain. Quantification of the monomer production in the brain is rather controversial in
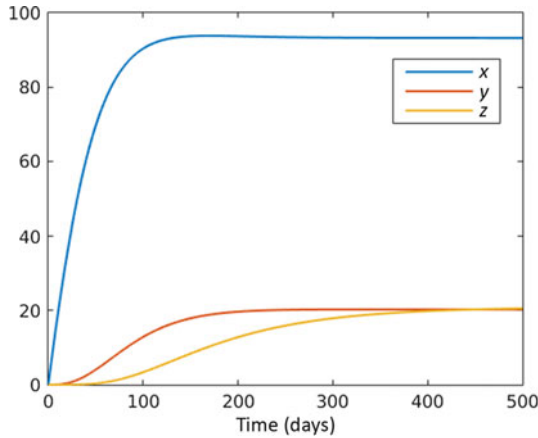
FIGURE 1. Solution of system (4.1) with $a = 0$.

the literature. For example, Karran et al. [39] mention an estimate of 4000 nanograms per day, whereas Bateman et al. [4] mention only 60 nanograms. In this context, our choice of λ_0 seems reasonable.

We choose the remaining constants in (4.1).

M_i Assuming that the daily clearance amounts to 1%, we take $M_i = 10^{-2}$ for $i = 1, 2, 3$.

k, k^* Although in the literature, there are various attempts to give explicit formulas for k and k^* [45, 49, 27], we believe that their choice remains rather arbitrary. In the simulations below, we choose $k = 10^{-4}$ and $k^* = 5 \times 10^{-6}$. In this context, we stress that our example is rather conceptual and speculative, and mainly aimed to illustrate the potentiality of the model.

Solving the system, for example, with initial data $X(0) = Y(0) = Z(0) = 0$ we find the solution when $a = 0$, displayed in Figure 1.

The graphs suggest that there exist equilibrium values reached within a few months even when the initial data are far from equilibrium. Referring to the Appendix for some additional comments on system (4.1), we just note that the system can be scaled: if the volume of the REV is divided by a factor m, then dividing λ by m and multiplying k and k^* by m, the asymptotic values of X, Y and Z are also divided by m.

4.1 Dynamics of AD: Local effect

Now we simulate the dynamics of AD. Assume that the threshold D^* (that in this particular case is a value Y^*) for the normalised number of toxic oligomers in a single REV is $Y^* = 22$.

First, we describe the degradation taking into account just the local effect based on (3.7). This is just a test of the model and would refer to the abstract situation in which the initial malfunctioning of the neurons affects all the REVs in the same way (thus canceling every prion-like transmission). We set $\theta = 10^{-3}$ and assume that at a given time (taken as $t = 0$), in each REV a jumps to a value 0.02 and therefore $\lambda = 2.548$. We take T as 180 days, that is, we update the value of a twice a year. The results are displayed in Figures 2, 3 and 4. More precisely,
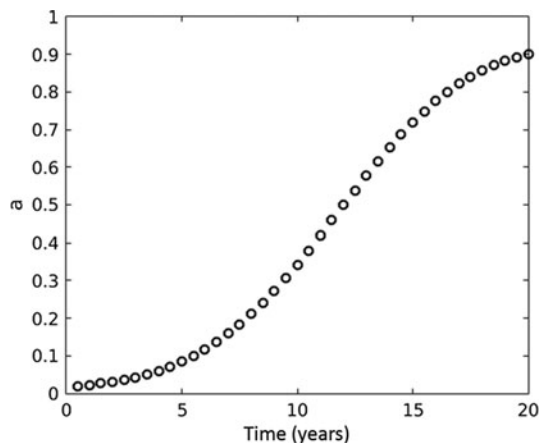
FIGURE 2. Progression of the average degradation a of neurons in an REV (local effect) when the onset of the disease takes place at $t = 0$ ($a(0) = 0.02$).
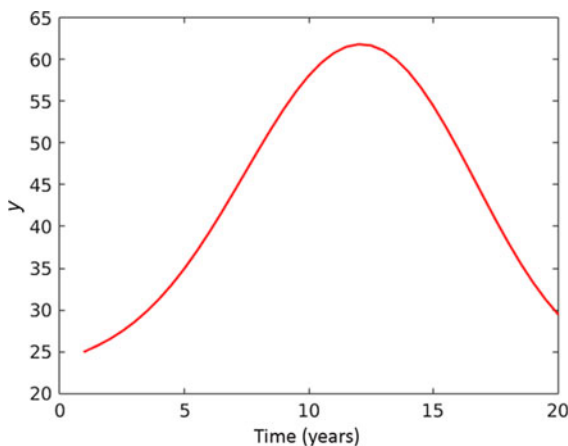

FIGURE 3. Evolution of the (normalised) number of toxic oligomers in the REV during the progression of the disease.

Figure 2 represents the evolution of the degradation a; Figure 3 shows the normalised number of toxic oligomers in each REV; Figure 4 shows how the production rate of monomers in each REV evolves with time. In these graphs, t is expressed in years after the onset of the disease. In the early stage of the disease, the shape of the curve appearing in Figures 3 and 4 fits the clinical data presented in the literature (see [37], Figure 6, and also [5], Figure 3). On the other hand, the decrease in the concentration of Aβ is well known in clinical practice: quoting from [3], 'meta-analyses suggest that AD can be differentiated from other dementias by the detection of lower concentration of Aβ_{1-42}...'. Moreover, low concentration of Aβ_{42} in CSF is listed among diagnostic criteria and differential diagnosis of AD from other dementias.

We point out that the stability of the model (more precisely of a similar model) is discussed in detail in [6].
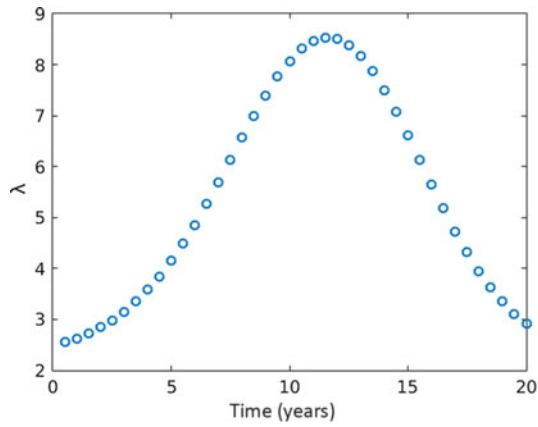
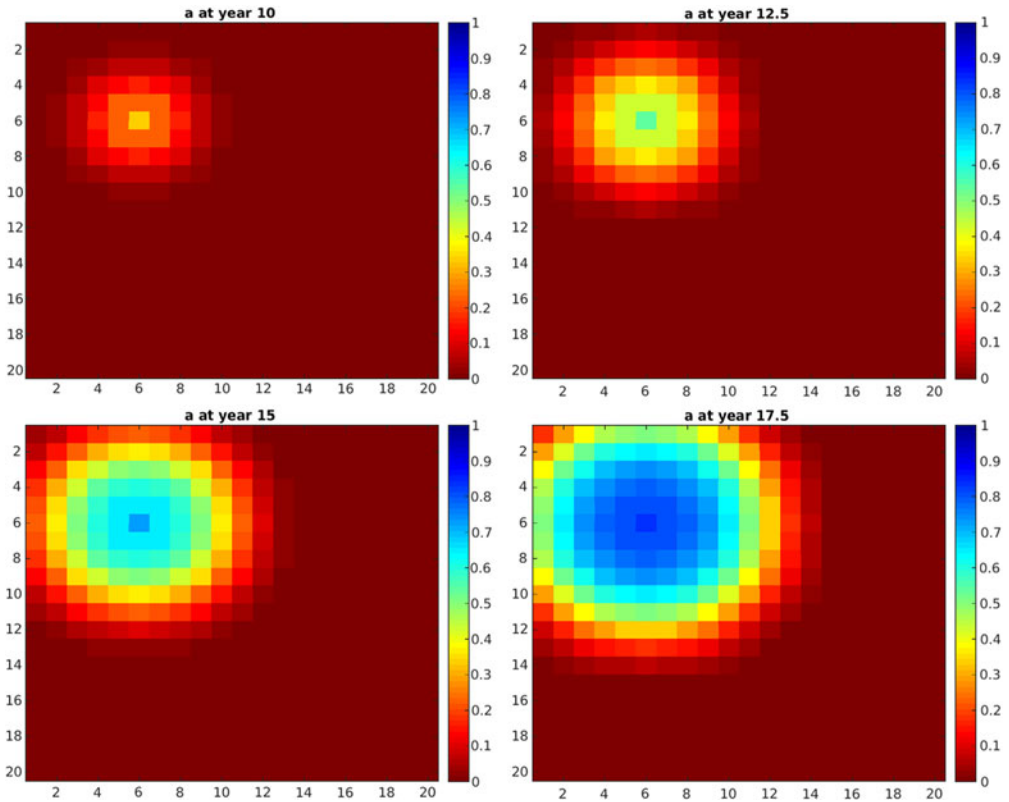FIGURE 4. Evolution of the average monomer production in the REV during the progression of the disease.

FIGURE 5. Non-local effect in a 2D model. Screenshots at different times ($t = 10, t = 12.5, t = 15, t = 17.5$ years). The initial situation is such that only one REV (of coordinates $(6, 6)$) has an initial malfunctioning index $a = 0.02$.
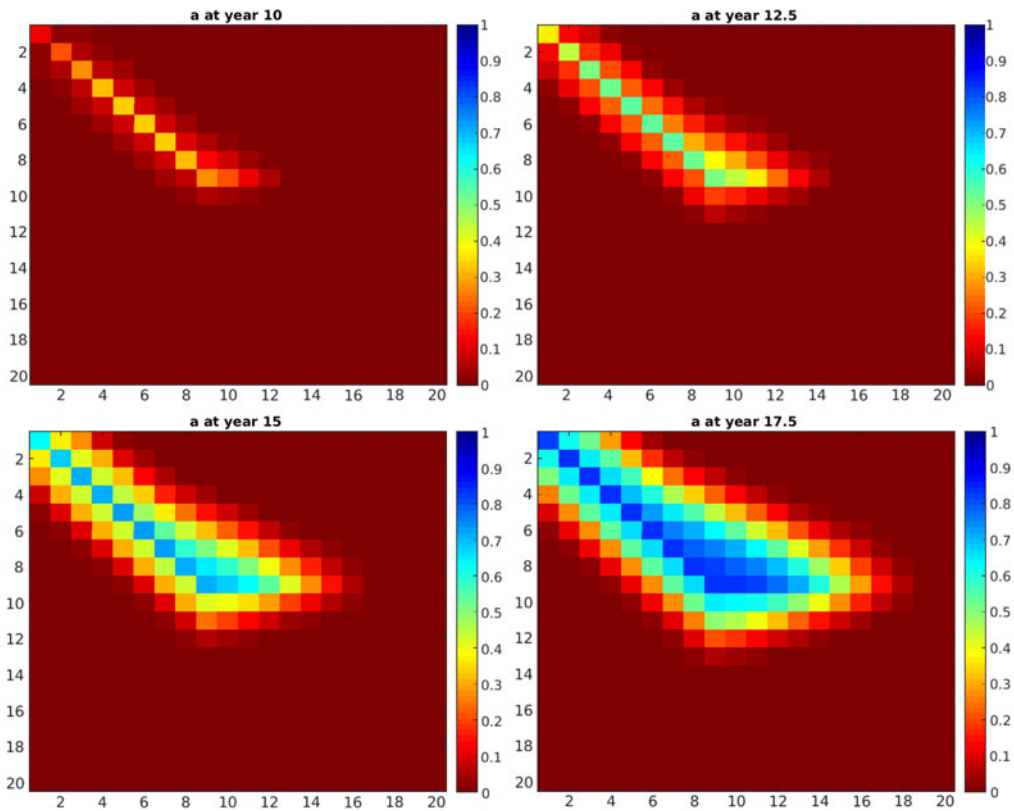
FIGURE 6. An example of non-isotropic propagation. Screenshots at different times ($t = 10, t = 12.5$, $t = 15, t = 17.5$ years). The initial situation is such that only one REV (of coordinates $(6, 6)$) has an initial malfunctioning index $a = 0.02$.

4.2 Including the non-local effect

To simplify the numerical simulation and the visualisation of the results, from now on we consider a 2D model: a square grid of 20×20 REVs. The setting of the parameters, for uniformity, will be the same as before: $M_i = 10^{-2}$, $k = 10^{-4}$ and $k^* = 5 \times 10^{-6}$. In addition to the local effect (3.7) (with $\theta = 10^{-3}$), we will take into account the prion-like propagation modelled by (3.8) starting with the case of isotropic propagation with $\sigma = 0.05$. As initial condition, we assume, for instance, that $a = 0$ in each REV with the exception of the square with coordinates $(6, 6)$, where we put $a = 0.02$. Figure 5, which contains the screenshots at 10, 12.5, 15 and 17.5 years, shows the progressive degradation of the tissue.

To conclude this section, we consider a case in which the propagation is anisotropic. In the following example case, we set the same initial condition of the previous example, that is, $a = 0.02$ in the region of coordinates $(6, 6)$ and $a = 0$ otherwise. But in this case, just to be specific, we assume that the propagation (corresponding to a value of $\sigma = 0.2$) in the directions NE–SW and E–W is 20 times larger than the propagation in the other directions, in the half-left-part and half-right-part of the brain, respectively. In Figure 6, we can see the particular behaviour of the propagation of the disease as visualised through the screenshots at 10, 12.5, 15 and 17.5 years.

5 Conclusions

We have proposed a relatively simple model for the so-called amyloid cascade hypothesis for AD and its effect on the state of degradation of neurons. Dividing a portion of the brain into sufficiently small subregions and averaging the state of degradation in each subregion, we have formulated a system of OEDs for the number of monomeric and oligomeric beta-amyloid polymers and the insoluble amyloid plaques. The typical timescale of the amyloid peptides evolution is much faster than that of the evolution of the state of degradation of the neurons. The latter process can take into account a prion-like diffusion of the disease. We have also presented some numerical results in 2D to illustrate the behaviour of the solutions. A MATLAB implementation of the mathematical model to simulate the results presented in this work is available in GitHub at the URL: https://github.com/LucaMeacci/Alzheimer_MathModel_Ejam.

The key point of the model is its high level of flexibility. Additional features could be implemented in the model. For instance,

- diffusion of soluble amyloid within the cerebral parenchyma;
- toxic effect of phosphorylated τ protein inside neurons and its interaction with β-amyloid;
- more realistic anatomy of the brain;
- clearance of the amyloid due to the continuous production and removal of the CSF.

The possibility of including different phenomena in the model is particularly important since the role of the various mechanisms in the development of AD is not yet well understood. In other words, numerical simulations can be used to test different modelling hypotheses.

Conflicts of interest

The authors have no conflicts of interest.

References

[1] ACHDOU, Y., FRANCHI, B., MARCELLO, N. & TESI, M. C. (2013) A qualitative model for aggregation and diffusion of β-amyloid in Alzheimer's disease. *J. Math. Biol.* **67**(6–7), 1369–1392.

[2] BACYINSKI, A., XU, M., WANG, W. & HU, J. (2017) The paravascular pathway for brain waste clearance: current understanding, significance and controversy. *Front Neuroanat.* **101**, 101.

[3] BALLARD, C., GAUTHIER, S., CORBETT, A., BRAYNE, C., AARSLAND, D. & JONES, E. (2011) Alzheimer's disease. *Lancet* **377**, 1019–1031.

[4] BATEMAN, R. J., MUNSELL, L. Y., MORRIS, J. C., SWARM, R., YARASHESKI, K. E. & HOLTZMAN, D. M. (2006) Quantifying CNS protein production and clearance rates in humans using in vivo stable isotope labeling, immunoprecipitation, and tandem mass spectrometry. *Nat. Med.* **12**(7), 856.

[5] BERTSCH, M., FRANCHI, B., MARCELLO, N., TESI, M. C. & TOSIN, A. (2017) Alzheimer's disease: a mathematical model for onset and progression. *Math. Med. Biol.* **34**(2), 193–214.

[6] BERTSCH, M., FRANCHI, B., MESCHINI, V., TESI, M. & TOSIN, A. (2020) A sensitivity analysis of a mathematical model for the synergistic interplay of Amyloid beta and tau on the dynamics of Alzheimer's disease. preprint, ArXiv: 2006.01749.

[7] BERTSCH, M., FRANCHI, B., TESI, M. & TOSIN, A. (2017) Microscopic and macroscopic models for the onset and progression of Alzheimer's disease. *J. Phys. A* **50**(41), 414003, 22.

[8] BERTSCH, M., FRANCHI, B., TESI, M. & TOSIN, A. (2018) Well-posedness of a mathematical model for Alzheimer's disease. *SIAM J. Math. Anal.* **50**(3), 2362–2388.

[9] BRAAK, H. & DEL TREDICI, K. (2011) Alzheimer's pathogenesis: is there neuron-to-neuron propagation? *Acta Neuropathol.* **121**(5), 589–595.

[10] CARBONELL, F., ITURRIA-MEDINA, Y. & EVANS, A. (2018) Mathematical modeling of protein misfolding mechanisms in neurological diseases: a historical overview. *Front. Neurol.* **9**(37), 1–16.

[11] CHEN, C. Y., TSENG, Y. H. & WARD, J. P. (2019) A mathematical model demonstrating the role of interstitial fluid flow on the clearance and accumulation of amyloid β in the brain. *Math. Biosci.* **317**, 108258.

[12] CHIMON, S., SHAIBAT, M., JONES, C., CALERO, D., AIZEZI, B. & ISHII, Y. (2007) Evidence of fibril-like β-sheet structures in a neurotoxic amyloid intermediate of Alzheimer's β-amyloid. *Nat. Struct. Mol. Biol.* **14**(12), 1157–1164.

[13] COHEN, A. D., RABINOVICI, G. D., MATHIS, C. A., JAGUST, W. J., KLUNK, W. E. & IKONOMOVIC, M. D. (2012) Using Pittsburgh compound b for in vivo pet imaging of fibrillar amyloid-beta. In: E. K. Michaelis and M. L. Michaelis (editors), *Current State of Alzheimer's Disease Research and Therapeutics*, Advances in Pharmacology, Vol. 64, Academic Press, pp. 27–81.

[14] CRAFT, D., WEIN, L. & SELKOE, D. (2002) A mathematical model of the impact of novel treatments on the a beta burden in the Alzheimer's brain, CSF and plasma. *Bull. Math. Biol.* **64**(5), 1011–1031.

[15] CRUZ, L., URBANC, B., BULDYREV, S. V., CHRISTIE, R., GÓMEZ-ISLA, T., HAVLIN, S., MCNAMARA, M., STANLEY, H. E. & HYMAN, B. T. (1997) Aggregation and disaggregation of senile plaques in Alzheimer disease. *P. Natl. Acad. Sci. USA* **94**(14), 7612–7616.

[16] DEACONU, M. & TANRÉ, E. (2000) Smoluchowski's coagulation equation: probabilistic interpretation of solutions for constant, additive and multiplicative kernels. *Ann. Scuola Norm. Sup. Pisa Cl. Sci. (4)* **29**(3), 549–579.

[17] DRAKE, R. (1972) A general mathematical survey of the coagulation equation. In: *Topics in Current Aerosol Research (Part 2), International Reviews in Aerosol Physics and Chemistry*, Pergamon Press, Oxford, UK, pp. 203–376.

[18] DUBOVSKII, P. B. (1994) *Mathematical Theory of Coagulation*, Lecture Notes Series, vol. 23, Seoul National University, Research Institute of Mathematics, Global Analysis Research Center, Seoul.

[19] EDELSTEIN-KESHET, L. & SPIROSS, A. (2002) Exploring the formation of Alzheimer's disease senile plaques in silico. *J. Theor. Biol.* **216**(3), 301–326.

[20] FORNARI, S., SCHAEFER, A., JUCKER, M., GORIELY, A. & KUHL, E. (2019) Prion-like spreading of Alzheimer's disease within the brain's connectome. *J. R. Soc. Interface* **159**, 20190356.

[21] FORNARI, S., SCHER, A., KUHL, E. & GORIELY, A. (2020) Spatially-extended nucleation-aggregation-fragmentation models for the dynamics of prion-like neurodegenerative protein-spreading in the brain and its connectome. *J. Theor. Biol.* **486**, 110102.

[22] FRANCHI, B., HEIDA, M. & LORENZANI, S. (2020) A mathematical model for Alzheimer's disease: an approach via stochastic homogenization of the Smoluchowski equation. *Commun. math. sci.*, **18**(4), 1105–1134.

[23] FRANCHI, B. & LORENZANI, S. (2016) From a microscopic to a macroscopic model for Alzheimer disease: two-scale homogenization of the Smoluchowski equation in perforated domains. *J. Nonlinear Sci.* **26**(3), 717–753.

[24] FRANCHI, B. & LORENZANI, S. (2017) Smoluchowski equation with variable coefficients in perforated domains: homogenization and applications to mathematical models in medicine. In: *Harmonic Analysis, Partial Differential Equations and Applications*, Appl. Numer. Harmon. Anal., Birkhäuser/Springer, Cham, pp. 49–67.

[25] FRANCHI, B. & TESI, M. (2012) A qualitative model for aggregation-fragmentation and diffusion of β-amyloid in Alzheimer's disease. *Rend. Semin. Mat. Univ. Politec. Torino* **70**(1), 75–84.

[26] FRIEDMAN, A. & HAO, W. (2016) Mathematical model on Alzheimer's disease. *BMC Syst. Biol.* **108**(10), 1–18.

[27] GILLAM, J. & MACPHEE, C. (2013) Modelling amyloid fibril formation kinetics: mechanisms of nucleation and growth. *J. Phys. Condens. Matter IOPScience* **25**(37), 373101.

[28] GIUFFRIDA, M. L., CARACI, F., PIGNATARO, B., CATALDO, S., DE BONA, P., BRUNO, V., MOLINARO, G., PAPPALARDO, G., MESSINA, A., PALMIGIANO, A., GAROZZO, D., NICOLETTI, F., RIZZARELLI, E. & COPANI, A. (2009) β-amyloid monomers are neuroprotective. *J. Neurosci.* **29**, 10582–10587.

[29] GOOD, T. A. & MURPHY, R. M. (1996) Effect of β-amyloid block of the fast-inactivating K^+ channel on intracellular Ca^{2+} and excitability in a modeled neuron. *P. Natl. Acad. Sci. USA* **93**, 15130–15135.

[30] GREER, M., PUJO-MENJOUET, L. & WEBB, G. (2006) A mathematical analysis of the dynamics of prion proliferation. *J. Theoret. Biol.* **242**(3), 598–606.

[31] GRIFFIN, W., SHENG, J., ROYSTON, M., GENTLEMAN, S., MCKENZIE, J., GRAHAM, D., ROBERTS, G. & MRAK, R. (1998) Glial-neuronal interactions in Alzheimer's disease: the potential role of a cytokine cycle in disease progression. *Brain Pathol.* **8**(1), 65–72.

[32] HAASS, C. & SELKOE, D. J. (2007) Soluble protein oligomers in neurodegeneration: lessons from the Alzheimer's amyloid beta-peptide. *Nat. Rev. Mol. Cell. Biol.* **8**(2), 101–112.

[33] HAHN, W. (1967) *Stability of Motion*. Translated from the German manuscript by Arne P. Baartz. Die Grundlehren der mathematischen Wissenschaften, Band 138, Springer-Verlag New York, Inc., New York.

[34] HELAL, M., HINGANT, E., PUJO-MENJOUET, L. & WEBB, G. F. (2013) Alzheimer's disease: analysis of a mathematical model incorporating the role of prions. *J. Math. Biol.* **69**(5), 1–29.

[35] HERRERO, M. A. & RODRIGO, M. (2005) A note on Smoluchowski's equations with diffusion. *Appl. Math. Lett.* **18**(9), 969–975.

[36] HURD, M. D., MARTORELL, P., DELAVANDE, A., MULLEN, K. J. & LANGA, K. M. (2013) Monetary costs of dementia in the United States. *New Engl. J. Med.* **368**(14), 1326–1334.

[37] JACK JR., C. R., KNOPMAN, D. S., JAGUST, W. J., SHAW, L. M., AISEN, P. S., WEINER, M. W., PETERSEN, R. C. & TROJANOWSKI, J. Q. (2013) Tracking pathophysiological processes in Alzheimer's disease: an updated hypothetical model of dynamic biomarkers. *Lancet Neurol.* **12**(2), 207–216.

[38] KAMETANI, F. & HASEGAWA, M. (2013) Reconsideration of amyloid hypothesis and tau hypothesis in Alzheimer's disease. *New Engl. J. Med.* **368**(14), 1326–1334.

[39] KARRAN, E., MERCKEN, M. & DE STROOPER, B. (2011) The amyloid cascade hypothesis for Alzheimer's disease: an appraisal for the development of therapeutics. *Nat Rev. Drug Discov.* **10**(9), 698–712.

[40] LAURENÇOT, P. & MISCHLER, S. (2002) Global existence for the discrete diffusive coagulation-fragmentation equations in L^1. *Rev. Mat. Iberoamericana* **18**(3), 731–745.

[41] MATTHUS, F. (2006) Diffusion versus network models as descriptions for the spread of prion diseases in the brain. *J. Theor. Biol.* **240**(1), 104–113.

[42] MEYER-LUEHMANN, M., SPIRES-JONES, T., PRADA, C., GARCIA-ALLOZA, M., DE CALIGNON, A., ROZKALNE, A., KOENIGSKNECHT-TALBOO, J., HOLTZMAN, D. M., BACSKAI, B. J. & HYMAN, B. T. (2008) Rapid appearance and local toxicity of amyloid-β plaques in a mouse model of Alzheimer's disease. *Nature* **451**(7179), 720–724.

[43] MOSCONI, L., BERTI, V., GLODZIK, L., PUPI, A., DE SANTI, S. & DE LEON, M. (2010) Pre-clinical detection of Alzheimer's disease using FDG-PET, with or without amyloid imaging. *J. Alzheimer's Dis.* **20**(3), 843–854.

[44] MOSES, W. (2011) Fundamental limits of spatial resolution in pet. *Nucl. Instrum. Methods Phys. Res. A.* **648**(Supplement 1), S236–S240.

[45] MURPHY, R. M. & PALLITTO, M. M. (2000) Probing the kinetics of β-amyloid self-association. *J. Struct. Biol.* **130**(2–3), 109–122.

[46] NAG, S., SARKAR, B., BANDYOPADHYAY, A., SAHOO, B., SREENIVASAN, V., KOMBRABAIL, M., MURALIDHARAN, C. & MAITI, S. (2011) Nature of the amyloid-β monomer and the monomer-oligomer equilibrium. *J. Biol. Chem.* **286**(16), 13827–13833.

[47] O'BRIEN, R. & WONG, P. (2011) Amyloid precursor protein processing and Alzheimer's disease. *Ann. Rev. Neurosci.* **34**(7), 185–204.

[48] ONO, K., CONDRON, M. M. & TEPLOW, D. B. (2009) Structure-neurotoxicity relationships of amyloid β-protein oligomers. *P. Natl. Acad. Sci. USA* **106**(35), 14745–14750.

[49] PALLITTO, M. M. & MURPHY, R. M. (2001) Mathematical model of the kinetics of beta-amyloid fibril growth from the denatured state. *Biophys. J.* **81**(3), 109–122.

[50] PARESCHI, L. & TOSCANI, G. (2013) *Interacting Multiagent Systems: Kinetic Equations and Monte Carlo Methods*, Oxford University Press, Oxford, UK.

[51] PLOG, B. & NEDERGAARD, M. (2018) The glymphatic system in central nervous system health and disease: past, present, and future. *Ann. Rev. Pathol. Mech. Dis.* **13**, 379–394.

[52] PRÜSS, J., PUJO-MENJOUET, L., WEBB, G. F. & ZACHER, R. (2006) Analysis of a model for the dynamics of prions. *Discrete Contin. Dyn. Syst. Ser. B* **6**(1), 225–235.

[53] RAJ, A., KUCEYESKI, A. & WEINER, M. (2012) A network diffusion model of disease progression in dementia. *Neuron* **73**(6), 1204–1215.

[54] RAJ, A., LOCASTRO, E., KUCEYESKI, A., TOSUN, D., RELKIN, N. & WEINER, M. (2015) Network diffusion model of progression predicts longitudinal patterns of atrophy and metabolism in Alzheimer's disease. *Cell Rep.* **10**(3), 359–369.

[55] SCHFER, A., WEICKENMEIER, J. & KUHL, E. (2019) The interplay of biochemical and biomechanical degeneration in Alzheimer's disease. *Comput. Methods Appl. Mech. Eng.* **352**, 369–388.

[56] SHANKAR, G. M., LI, S., MEHTA, T. H., GARCIA-MUNOZ, A., SHEPARDSON, N. E., SMITH, I., BRETT, F. M., FARRELL, M. A., ROWAN, M. J., LEMERE, C. A., REGAN, C. M., WALSH, D. M., SABATINI, B. L. & SELKOE, D. J. (2008) Amyloid-beta protein dimers isolated directly from Alzheimer's brains impair synaptic plasticity and memory. *Nat. Med.* **14**, 837–842.

[57] SMOLUCHOWSKI, M. (1917) Versuch einer mathematischen theorie der koagulationskinetik kolloider lsungen. *IZ. Phys. Chem.* **92**, 129–168.

[58] TATARNIKOVA, O. G., ORLOV, M. A. & BOBKOVA, N. V. (2015) Beta-amyloid and tau protein: structure, interaction and prion-like properties. *Biochemistry (Moscow)* **80**(13), 1800–1819.

[59] URBANC, B., CRUZ, L., BULDYREV, S. V., HAVLIN, S., IRIZARRY, M. C., STANLEY, H. E. & HYMAN, B. T. (1999) Dynamics of plaque formation in Alzheimer's disease. *Biophys. J.* **76**(3), 1330–1334.

[60] WALSH, D. M. & SELKOE, D. J. (2007) Aβ oligomers: a decade of discovery. *J. Neurochem.* **101**(5), 1172–1184.

[61] WEICKENMEIER, J., JUCKER, M., GORIELY, A. & KUHL, E. (2019) A physics-based model explains the prion-like features of neurodegeneration in Alzheimer's disease, Parkinson's disease, and amyotrophic lateral sclerosis. *J. Mech. Phys. Solids* **124**, 264–281.

[62] WRZOSEK, D. (1997) Existence of solutions for the discrete coagulation-fragmentation model with diffusion. *Topol. Methods Nonlinear Anal.* **9**(2), 279–296.

[63] Zou, K., Gong, J. S., Yanagisawa, K. & Michikawa, M. (2002) A novel function of monomeric amyloid-protein serving as an antioxidant molecule against metal-induced oxidative damage. *J. Neurosci.* **22**, 4833–4841.

A Appendix

A.1 Global existence of solutions of system (4.1)

We consider the system (4.1) with positive initial data $X(0), Y(0), Z(0)$. It is easy to show that the system has a global positive solution. Indeed, we show that X, Y and Z are bounded. For this purpose, we consider the system

$$
\begin{cases}
X' = -kX^2 - kXY - k^*XZ - M_1 X + \lambda \\
Y' = \frac{1}{2}kX^2 - kXY - kY^2 - k^*YZ - M_2 Y \\
Z' = \frac{1}{2}kY^2 + kXY - M_3 Z,
\end{cases}
$$

with positive Cauchy data $X(0), Y(0), Z(0)$. Then $X(t) > 0$, $Y(t) > 0$, $Z(t) > 0$ as long as the solution exists.

In addition

$$
X' \le -kX^2 + \lambda - k^*XZ \Rightarrow X(t) \le \alpha := \max\left\{ X(0), \sqrt{\frac{\lambda}{k}} \right\}
$$

$$
Y' \le k\alpha^2 - kY^2 - k^*YZ \Rightarrow Y(t) \le \beta := \max\{Y(0), \alpha\}
$$

$$
Z' \le \frac{1}{2}k\beta^2 + k\alpha\beta - M_3 Z,
$$

so that also Z is bounded.

A.2 Equilibrium solutions

Let us consider the *equilibrium solutions* of system (4.1), that is, the solutions of the algebraic system

$$
\begin{cases}
0 = -kX^2 - kXY - k^*XZ - M_1 X + \lambda \\
0 = \frac{1}{2}kX^2 - kXY - kY^2 - k^*YZ - M_2 Y \\
0 = \frac{1}{2}kY^2 + kXY - M_3 Z.
\end{cases}
\tag{A1}
$$

We shall prove that system (4.1) has an equilibrium solution

$$
X \equiv X_0 > 0 \qquad Y \equiv Y_0 > 0 \qquad Z \equiv Z_0 > 0.
\tag{A2}
$$

In addition, this solution is unique among all positive equilibrium solutions of (A1).

Existence of equilibrium solutions: Solutions of system (A1) satisfy $Z = \frac{k}{2M_3}Y^2 + \frac{k}{M_3}XY$ and

$$
\begin{cases}
-kX^2 - kXY - k^*X\left(\frac{k}{2M_3}Y^2 + \frac{k}{M_3}XY\right) - M_1 X + \lambda = 0 \\
\frac{1}{2}kX^2 - kXY - kY^2 - k^*Y\left(\frac{k}{2M_3}Y^2 + \frac{k}{M_3}XY\right) - M_2 Y = 0,
\end{cases}
$$

that is, a system of 2 quadratic equations in X:

$$\begin{cases} \left(1 + \frac{k^*}{M_3}Y\right)X^2 + \left(Y + \frac{k^*}{2M_3}Y^2 + \frac{M_1}{k}\right)X - \frac{\lambda}{k} = 0 \\ X^2 - 2\left(Y + \frac{k^*}{M_3}Y^2\right)X - 2Y^2 - \frac{k^*}{M_3}Y^3 - \frac{2M_2}{k}Y = 0. \end{cases}$$

The positive solutions of the quadratic equations are

$$X = X_1(Y) = \frac{-\left(Y + \frac{k^*}{2M_3}Y^2 + \frac{M_1}{k}\right) + \sqrt{\left(Y + \frac{k^*}{2M_3}Y^2 + \frac{M_1}{k}\right)^2 + \frac{4\lambda}{k}\left(1 + \frac{k^*}{M_3}Y\right)}}{2\left(1 + \frac{k^*}{M_3}Y\right)}$$

and

$$X = X_2(Y) = Y + \frac{k^*}{M_3}Y^2 + \sqrt{\left(Y + \frac{k^*}{M_3}Y^2\right)^2 + 2Y^2 + \frac{k^*}{M_3}Y^3 + \frac{2M_2}{k}Y}.$$

Observe that $X_2(Y)$ is strictly increasing,

$$X_2(0) = 0, \qquad X_2(\infty) = \infty, \qquad X_1(0) = -\frac{M_1}{2k} + \frac{1}{2}\sqrt{\left(\frac{M_1}{k}\right)^2 + \frac{4\lambda}{k}} > 0,$$

and

$$\begin{aligned} X_1(Y) &= \frac{Y + \frac{k^*}{2M_3}Y^2 + \frac{M_1}{k}}{2\left(1 + \frac{k^*}{M_3}Y\right)}\left(-1 + \sqrt{1 + \frac{\frac{4\lambda}{k}\left(1 + \frac{k^*}{M_3}Y\right)}{\left(Y + \frac{k^*}{2M_3}Y^2 + \frac{M_1}{k}\right)^2}}\right) \\ &= \frac{Y + \frac{k^*}{2M_3}Y^2 + \frac{M_1}{k}}{2\left(1 + \frac{k^*}{M_3}Y\right)}\left(\frac{\frac{4\lambda}{k}\left(1 + \frac{k^*}{M_3}Y\right)}{2\left(Y + \frac{k^*}{2M_3}Y^2 + \frac{M_1}{k}\right)^2}\right)(1 + o(1)) \to 0 \quad \text{as } Y \to \infty. \end{aligned}$$

Hence, the curves $X = X_1(Y)$ and $X = X_2(Y)$ have at least one intersection point (X_0, Y_0), which corresponds to an equilibrium solution (X_0, Y_0, Z_0), where $Z_0 = \frac{k}{2M_3}Y_0^2 + \frac{k}{M_3}X_0Y_0$.

Uniqueness of equilibrium solutions: Let us notice preliminarily that a solution (X_0, Y_0, Z_0) of system (A1) such that $X_0 > 0, Y_0 > 0, Z_0 > 0$ satisfies (A2).

The last equation gives

$$M_3 Z = \frac{1}{2}kY^2 + kXY.$$

Replacing in (A1), we have

$$\begin{cases} 0 = -kX^2 - kXY - \frac{k^*}{M_3}X\left(\frac{1}{2}kY^2 + kXY\right) - M_1X + \lambda \\ 0 = \frac{1}{2}kX^2 - kXY - kY^2 - \frac{k^*}{M_3}Y\left(\frac{1}{2}kY^2 + kXY\right) - M_2Y \qquad \text{(A3)} \\ 0 = \frac{1}{2}kY^2 + kXY - M_3Z. \end{cases}$$

Multiplying the first equation by $-Y$ and the second by X, we obtain

$$\begin{cases} 0 = kX^2Y + kXY^2 + \frac{k^*}{M_3}XY\left(\frac{1}{2}kY^2 + kXY\right) + M_1XY - \lambda Y \\ 0 = \frac{1}{2}kX^3 - kX^2Y - kXY^2 - \frac{k^*}{M_3}XY\left(\frac{1}{2}kY^2 + kXY\right) - M_2YX \\ 0 = \frac{1}{2}kY^2 + kXY - M_3Z. \end{cases} \quad (A4)$$

Summing up the two first equations in (A4), we get

$$\begin{aligned} \lambda Y &= kX^2Y + kXY^2 + \frac{kk^*}{2M_3}XY^3 + \frac{kk^*}{M_3}X^2Y^2 + M_1XY \\ &\quad + \frac{1}{2}kX^3 - kX^2Y - kXY^2 - \frac{kk^*}{2M_3}XY^3 - \frac{kk^*}{M_3}X^2Y^2 - M_2YX, \end{aligned} \quad (A5)$$

and eventually

$$Y\left(\lambda + (M_2 - M_1)X\right) = \frac{k}{2}X^3.$$

Since $X > 0$, necessarily, $\lambda + (M_2 - M_1)X > 0$. Consider now the function

$$f(X) = \frac{\frac{k}{2}X^3}{\lambda + (M_2 - M_1)X},$$

defined on the interval

$$I := \{X > 0, \ \lambda + (M_2 - M_1)X > 0\}.$$

We notice now that $f'(X) > 0$ in I, since

$$\begin{aligned} \frac{3k}{2}X^2\left(\lambda + (M_2 - M_1)X\right) &- \frac{k}{2}X^3(M_2 - M_1) \\ &= kX^3(M_2 - M_1) + \frac{3k\lambda}{2}X^2 = kX^2\left(X(M_2 - M_1) + \frac{3\lambda}{2}\right) \\ &> \frac{\lambda}{2} > 0. \end{aligned}$$

Thus, by contradiction, if (X_0, Y_0, Z_0) and (X_1, Y_1, Z_1) are different solutions of (A1) with $0 < X_0 < X_1$, we have $0 < Y_0 < Y_1$. Then the first equation of (A3) gives

$$\begin{aligned} \lambda &= kX_0^2 + kX_0Y_0 + \frac{k^*}{M_3}X_0\left(\frac{1}{2}kY_0^2 + kX_0Y_0\right) + M_1X_0 \\ &< kX_1^2 + kX_1Y_1 + \frac{k^*}{M_3}X_1\left(\frac{1}{2}kY_1^2 + kX_1Y_1\right) + M_1 = \lambda, \end{aligned}$$

yielding a contradiction.

To be specific, we substitute the values $M_i = 10^{-2}$, $k = 10^{-4}$ and $k^* = 5 \times 10^{-6}$, as in our simulations and we find that $X_1(Y)$ is decreasing and that the intersection of the two curves $X = X_1(Y)$ and $X = X_2(Y)$ corresponds to the values found in Figure 1 of Section 4, as it can be seen in Figure A.1.

Stability of equilibrium solutions: For sake of simplicity, from now on we assume $M_1 = M_2 = M_3 =: M$. In order to prove the asymptotic stability of the equilibrium solution, we have to prove that the eigenvalues of the Jacobian matrix
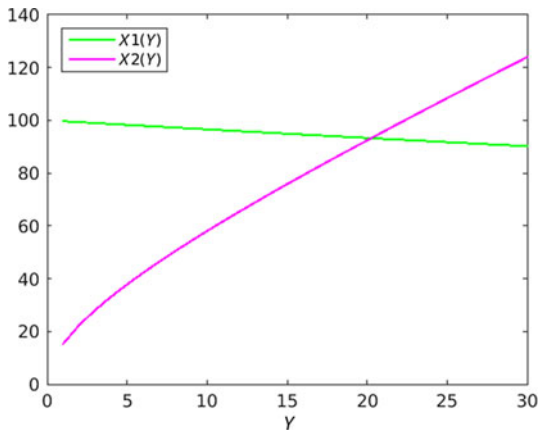
FIGURE A.1. Graphs of the curves $X = X_1(Y)$ and $X = X_2(Y)$ with $M_i = 10^{-2}$, $k = 10^{-4}$ and $k^* = 5 \times 10^{-6}$.

$$\begin{pmatrix} -2kX - kY - k^*Z - M & -kX & -k^*X \\ kX - kY & -kX - 2kY - k^*Z - M & -k^*Y \\ kY & kX + kY & -M \end{pmatrix} \tag{A6}$$

of the map defined by (A1), evaluated at the critical point (X, Y, Z), have negative real parts, keeping in mind that $X > 0$, $Y > 0$, $Z > 0$. In other words, we have to prove that the characteristic polynomial of the Jacobian matrix of (A1) is a so-called Hurwitz polynomial (see, e.g., [33], Chapter II, Theorem 4.2). We write the characteristic polynomial in the form

$$-\lambda^3 + a\lambda^2 + b\lambda + c. \tag{A7}$$

An elementary computation shows that $c < 0$, so that the polynomial (A7) has a real negative solution. In order to prove that the remaining solutions have negative real part, we apply to (A7) the so-called Routh–Hurwitz criterion (see, e.g., [33], Chapter II, Theorem 6.1). It is straightforward to see that $a < 0$, $b < 0$, so that we have but to show (see equation (6.1) in [33]) that

$$ab + c > 0. \tag{A8}$$

A cumbersome but elementary computation shows now that

$$\begin{aligned} ab + c = {}& k^2(9k - k^*)X^3 + 21k^3X^2Y + 18k^3XY^2 + 6k^3Y^3 + 3k^2k^*X^2Y \\ & + 15k^2k^*X^2Z + 6k^2k^*XY^2 + 26k^2k^*XYZ \\ & + 2k^2k^*Y^3 + 13k^2k^*Y^2Z + 24k^2MX^2 + 44k^2MXY + 22k^2MY^2 + 2kk^{*2}XYZ \\ & + 9kk^{*2}XZ^2 + kk^{*2}Y^2Z + 9kk^{*2}YZ^2 + 4kk^*MXY \\ & + 30kk^*MXZ + 2kk^*MY^2 + 30kk^*MYZ + 24kM^2X + 24kM^2Y \\ & + 2k^{*3}Z^3 + 10k^{*2}MZ^2 + 16k^*M^2Z + 8M^3 > 0, \end{aligned}$$

provided $k \geq \frac{1}{9}k^*$.

Table A.1. *Dependence of $\hat{Y}$ on the values chosen for k*

k	$\hat{Y}$
10^{-4}	20.26
0.5×10^{-4}	20.51
2×10^{-4}	18.00

Table A.2. *Dependence of $\hat{Y}$ on the values chosen for M*

M	$\hat{Y}$
10^{-2}	20.26
0.5×10^{-2}	29.62
2×10^{-2}	9.06

Thus, the equilibrium solution of the system (A1) with positive Cauchy data is asymptotically stable when $k \geq \frac{1}{9}k^*$. This condition is coherent with the choice of k, k^* in Figure A.1, that is, $k^* = \frac{k}{20}$.

A.3 Parameter dependence

Here, we sketch a numerical investigation on the dependence of the model on the values chosen for the parameters k and M_i. In particular, we show how their variations influence the values of the asymptotic value of Y (that will be denoted by $\hat{Y}$) which is the key factor in the evolution of AD.

We have already noted that multiplying k and k^* by a factor m and dividing λ by the same factor, then X, Y and Z are also divided by m. Maintaining the same relationship between k and k^* as in our simulations ($k^* = k/20$) we see that doubling or dividing by 2 the value of k does not induce a relevant variation in $\hat{Y}$ (see Table A.1).

On the other hand, as evident from the data in Table A.2, the dependence on M (which, as in our simulations, is the common value of M_1, M_2 and M_3) is much more critical.